Supporting Information

TiO$_2$-Enhanced *in situ* Electrochemical Activation of Co$_3$O$_4$ for the Alkaline Hydrogen Evolution Reaction

Ling Yuan, [#a] Danil W. Boukhvalov, [#bc] Cuncai Lv,[d] Jie Dong,[a] Tong He,[a] Zhiyang Yu,[e] Wenjie Luo,[f] Chuanwei Cheng,[f] Mark G. Humphrey,[g] Chi Zhang,*[a] Zhipeng Huang*[a]

[a] School of Chemical Science and Engineering, Tongji University, Shanghai, 200092, P.R. China

[b] Jiangsu Co-Innovation Center of Efficient Processing and Utilization of Forest Resources, College of Science, Nanjing Forestry University, Nanjing 210037, PR China

[c] Institute of Physics and Technology, Ural Federal University, Mira Str. 19 620002 Yekaterinburg, Russia

[d] Key Laboratory of High-precision Computation and Application of Quantum Field Theory of Hebei Province, Hebei Key Lab of Optic-electronic Information and Materials, The College of Physics Science and Technology, Hebei University, Baoding 071002, PR China

[e] State Key Laboratory of Photocatalysis on Energy and Environment, College of Chemistry, Fuzhou University, Fuzhou, 350002, P. R. China

[f] Shanghai Key Laboratory of Special Artificial Microstructure Materials and Technology, School of Physics Science and Engineering, Tongji University, Shanghai 200092, PR China

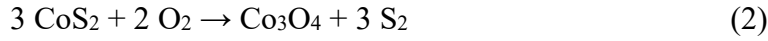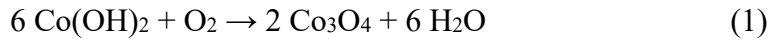[g] Research School of Chemistry, Australian National University, Canberra, ACT 2601, Australia

# Equal contribution
* Corresponding author.
E-mail: zphuang@tongji.edu.cn, chizhang@tongji.edu.cn

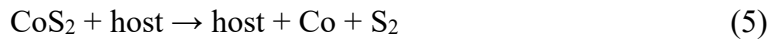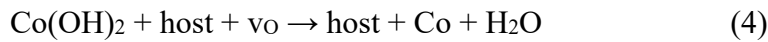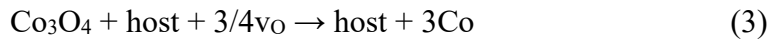**DFT 1. Enthalpies of Co(OH)$_2$ and CoS$_2$ oxidation.**

We have calculated enthalpies of two further reactions:

$$6\ Co(OH)_2 + O_2 \rightarrow 2\ Co_3O_4 + 6\ H_2O \qquad (1)$$

$$3\ CoS_2 + 2\ O_2 \rightarrow Co_3O_4 + 3\ S_2 \qquad (2)$$

The equations above correspond with realistic pathways for transformation of Co(OH)$_2$ and CoS$_2$ in the presence of oxygen during TiO$_2$ deposition. The values of the enthalpies were calculated as the differences of the sums of total energies of products and reactants.

DFT 2. Formation energies of Co-defects.

For all considered titanium dioxide hosts (*i.e.* d-TiO$_2$, a-TiO$_x$, and TiO$_2$), we explored incorporation of cobalt impurities from different sources (*i.e.* Co$_3$O$_4$, Co(OH)$_2$, CoS$_2$) as further reactions:

$$Co_3O_4 + host + 3/4v_O \rightarrow host + 3Co \qquad (3)$$

$$Co(OH)_2 + host + v_O \rightarrow host + Co + H_2O \qquad (4)$$

$$CoS_2 + host \rightarrow host + Co + S_2 \qquad (5)$$

Decomposition of Co$_3$O$_4$ and Co(OH)$_2$ is considered as corresponding with the healing of the oxygen vacancies (v$_O$) in bulk TiO$_2$.

DFT 3. Modified model of the Volmer step.

In contrast to the HER in acidic media, where the process $2H^+ + 2e^- \rightarrow H_2$ can be described through a combination of Volmer-Heyrovsky or Volmer-Tafel steps, in alkaline media the process is more complicated. The overall reaction can be described by the further equation:

$$2\ H_2O + 2e^- \rightarrow H_2 + 2\ OH^- \qquad (6)$$

Usually, reaction (1) is discussed as two steps. The first step is the decomposition of water with adsorption of hydrogen on a catalytic substrate (s1)

$$H_2O \rightarrow s1\text{-}H^+ + OH^- \qquad (7)$$

and the second step is the Heyrovsky or Tafel reaction, as in the case of HER in acidic media. The main disadvantage of the proposed reaction pathway is the high energy cost of the formation of free OH$^-$. The overall energy cost of reaction (6) can be decreased by the large negative enthalpy of formation of the s1-H$^+$ structure, but in this case desorption of hydrogen

will be energetically unfavorable. In our recent work, we proposed alternative scenarios for the reaction, described in equation (7):[1]

$$H_2O \rightarrow s1\text{-}H^+ + s1\text{-}OH^- \qquad\qquad (8') \text{ or}$$

$$H_2O \rightarrow s1\text{-}H^+ + s2\text{-}OH^-, \qquad\qquad (8'')$$

where s2 is another catalytic substrate (co-catalyst). In scenarios proposed in equations 8' and 8'', the energy cost for the formation of free OH^- is decreased by the intermediate adsorption of the hydroxyl group on the surface of the catalyst or co-catalyst.

Table S1. Comparison of the binding energies of metals in HER electrocatalysts to those of zero valence state and those in the oxide.

Metal / Nonmetal	Zero valence	Boride	Carbide	Nitride	Phosphide	Sulfide	Selenide	Oxide
Mo	Mo^2	MoB^3	Mo_2C^3	Mo_2N^4	MoP^5	MoS_2^6	$MoSe_2^7$	MoO_3^8
3d5/2	227.4	227.7	227.7	228.9	228.8	228.6	228.6	232.2
W	W^9	WB^{10}	WC^{11}	WN^{12}	WP^{13}	WS_2^{14}	WSe_2^{15}	WO_3^{16}
4f7/2	30.7	31.56	31.4	31.9	31.5	31.8	32.1	34.7
Fe	Fe^{17}	FeB_2^{18}	Fe_3C^{19}	Fe_2N^{20}	FeP^{21}	FeS_2^{22}	$FeSe_2^{23}$	$Fe_2O_3^{24}$
2p3/2	706.5	707.1	706.9	707.1	707.2	707.0	706.64	709.9
Co	Co^{25}	Co_2B^{26}	Co_3C^{19}	CoN^{27}	CoP^{28}	CoS_2^{29}	$CoSe_2^{30}$	CoO^{31}
2p3/2	777.8	778.5	778.4	779.0	778.6	778.8	778.4	780.2
Ni	Ni^{32}	NiB_x^{33}	Ni_3C^{19}	Ni_3N^{34}	$Ni_{12}P_5^{35}$	NiS_2^{36}	$NiSe_2^{37}$	NiO^{38}
2p3/2	852.0	852.8	853.3	853.1	853.1	852.9	853.3	854.4

The second column of **Table S1** shows the binding energies of zero valence species of metal, and the last column shows the binding energies of metal species in the oxide. The data in columns 3 to 8 comes from the references that introduced the HER activity of the corresponding compound.

The chemical shifts of metal species in the HER electrocatalysts, *e.g.* borides (column 3), carbides (column 4), nitrides (column 5), phosphides (column 6), sulfides (column 7), and selenides (column 8), are in the range 0.3 ~ 1.3 eV. while those in the corresponding oxides are much larger (3 ~ 5 eV). It is therefore suggested that the metal species in these HER electrocatalysts are partially charged.
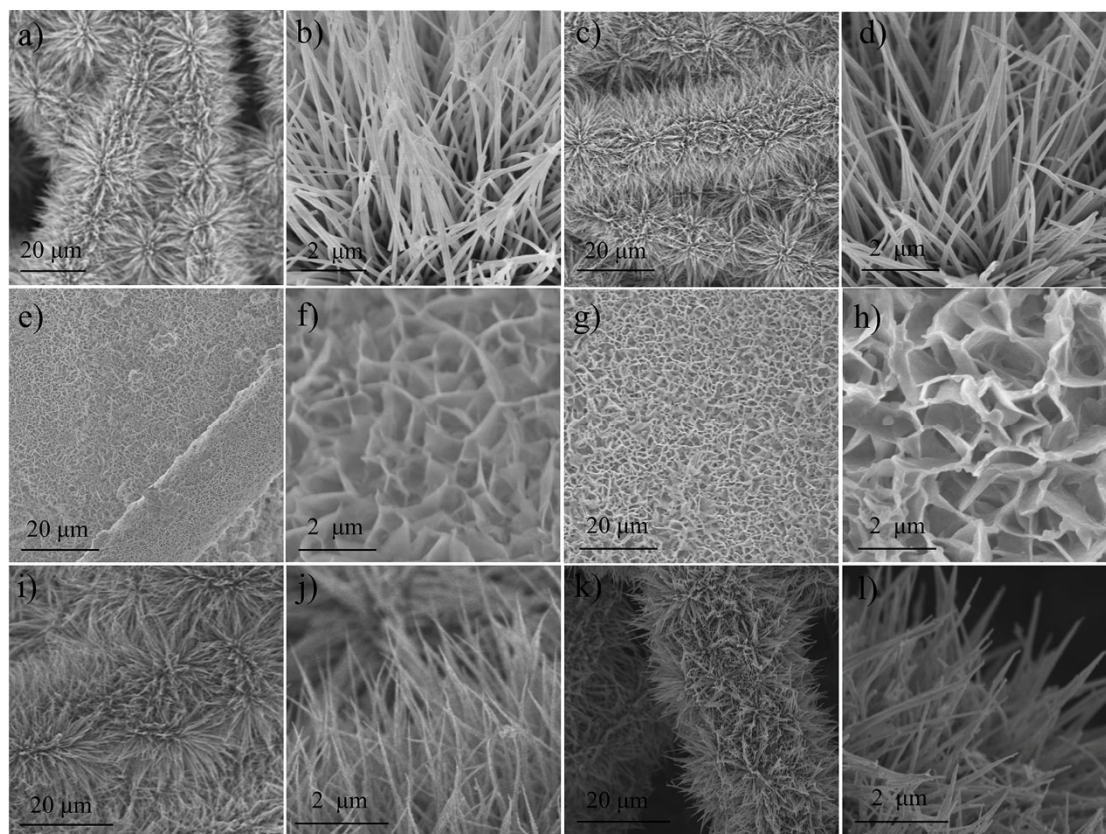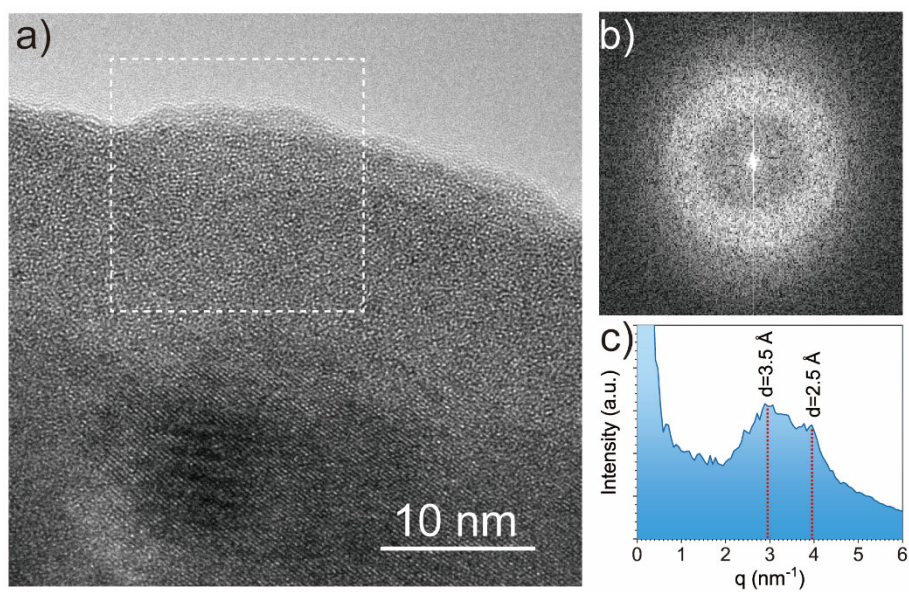
Figure S1. SEM images of (a,b) Co_3O_4, (c,d) $TiO_2@Co_3O_4$, (e,f) $Co(OH)_2$, (g,h) $TiO_2@Co(OH)_2$, (i,j) CoS_2, and (k,l) $TiO_2@CoS_2$.
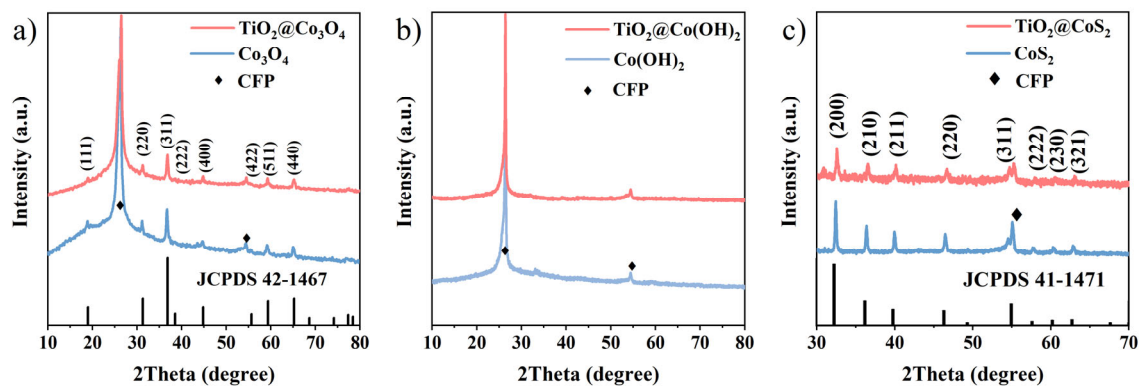
Figure S2. XRD patterns of (a) Co_3O_4 and $TiO_2@Co_3O_4$, (b) $Co(OH)_2$ and $TiO_2@Co(OH)_2$, and (c) CoS_2 and $TiO_2@CoS_2$.
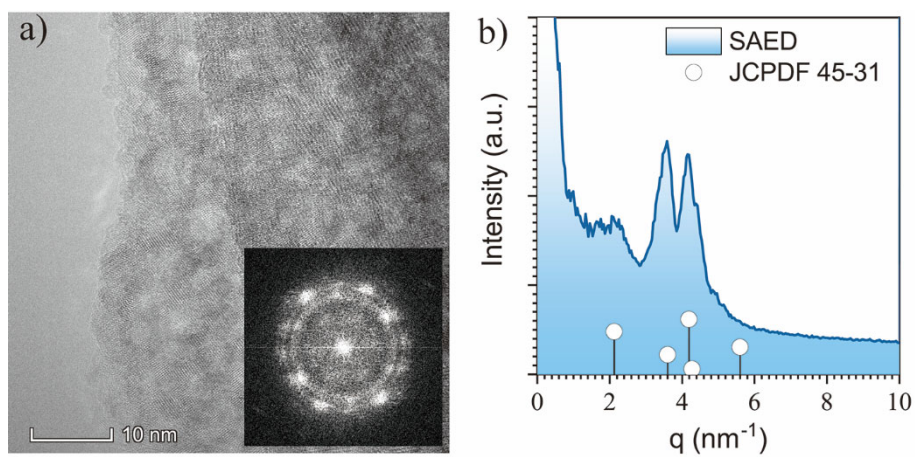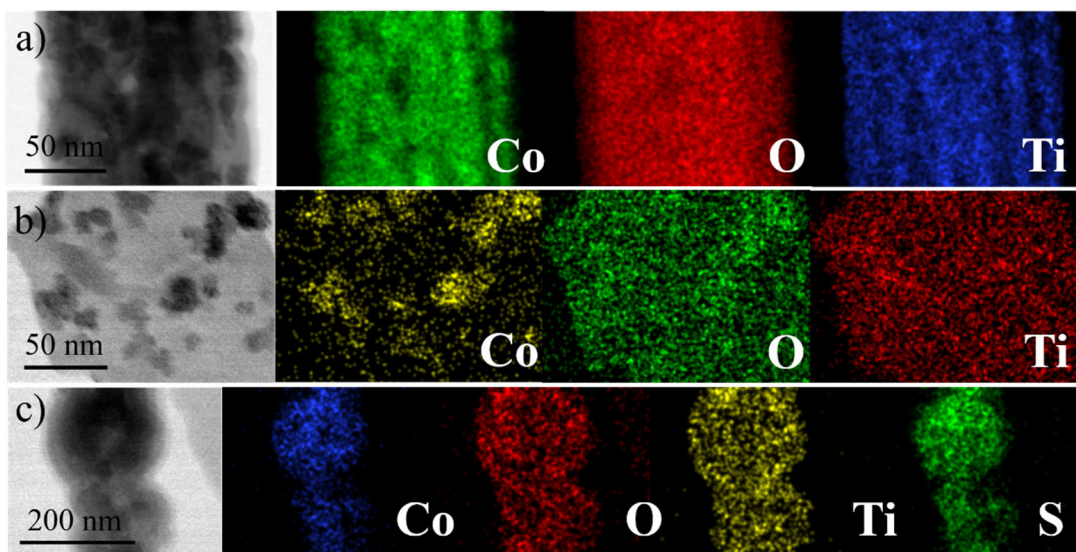
Figure S3. (a) High magnification TEM image and corresponding FFT pattern (inset) of Co(OH)$_2$. (b) Radial intensity profile of the FFT pattern.
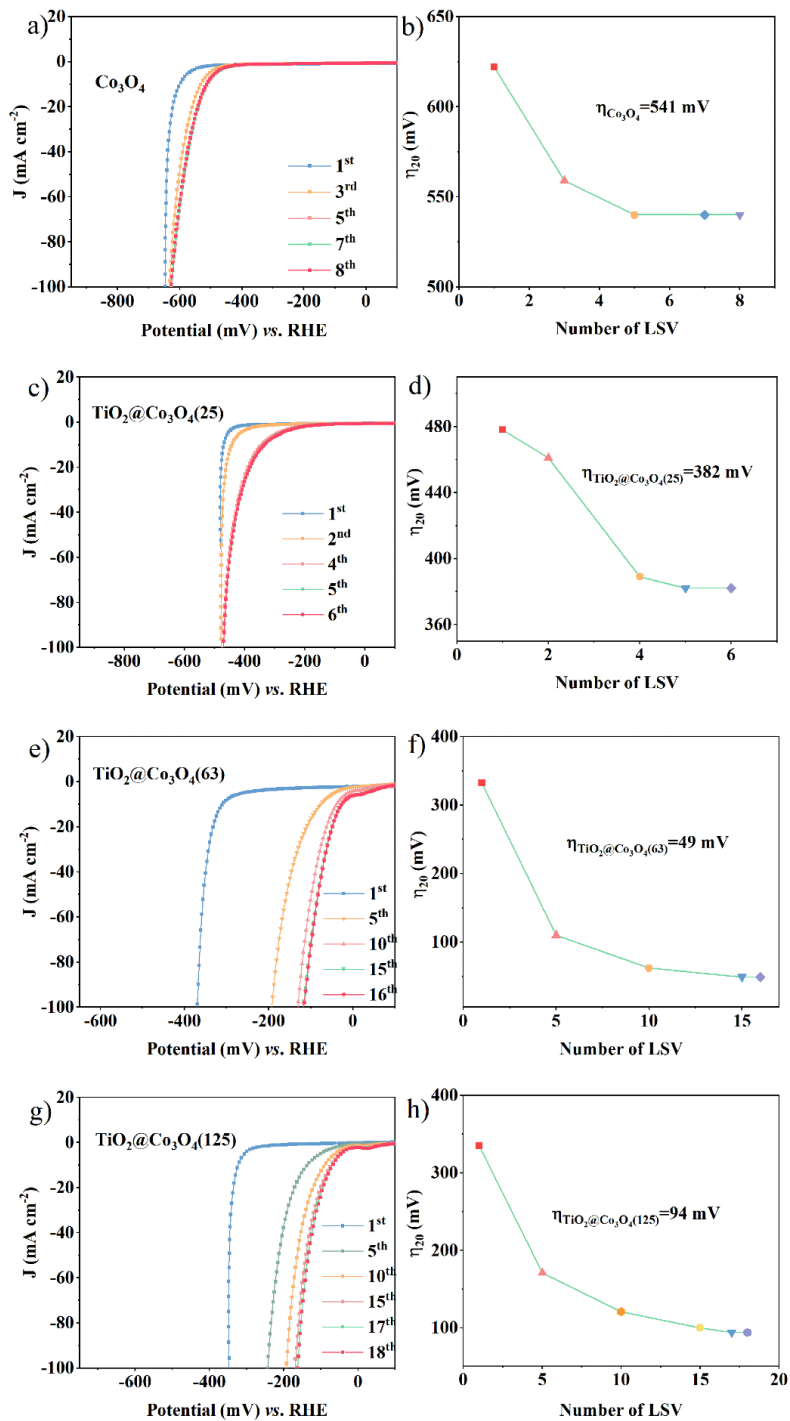
Figure S4. (a) TEM image of the TiO_2 coating on the surface of Co_3O_4. The rectangle encloses a TiO_2 region. (b) FFT pattern of a region enclosed by the square in (a). (c) Radial intensity profile of FFT patterns in (b).

Figure S5. STEM images and corresponding EDS mapping of (a) $TiO_2@Co_3O_4$, (b) $TiO_2@Co(OH)_2$, and (c) $TiO_2@CoS_2$.

Figure S6. LSV curves of (a) pristine Co₃O₄, (c) TiO₂@Co₃O₄(25), (e) TiO₂@Co₃O₄(63), and (g) TiO₂@Co₃O₄(125). Variation of η_{20} with the number of LSV scans corresponding to (b) pristine Co₃O₄, (e) TiO₂@Co₃O₄(25), (f) TiO₂@Co₃O₄(63), and (h) TiO₂@Co₃O₄(125). The number in the brackets following the name of the compounds is the ALD deposition cycle number.
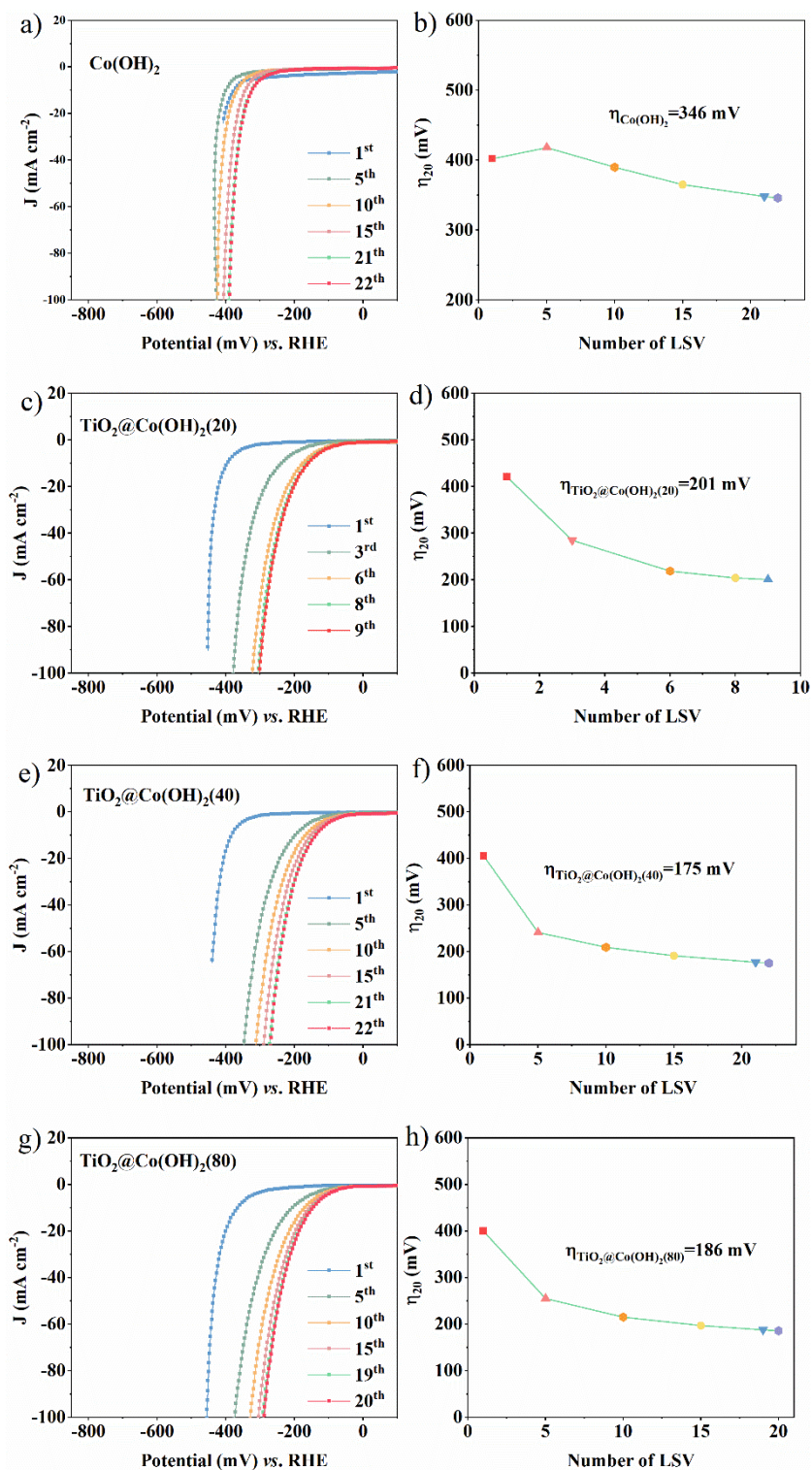
Figure S7. Activation process for Co(OH)$_2$, TiO$_2$@Co(OH)$_2$(20), TiO$_2$@Co(OH)$_2$(40), and TiO$_2$@Co(OH)$_2$(80). The number in the brackets following the name of compounds is the ALD deposition cycle number.
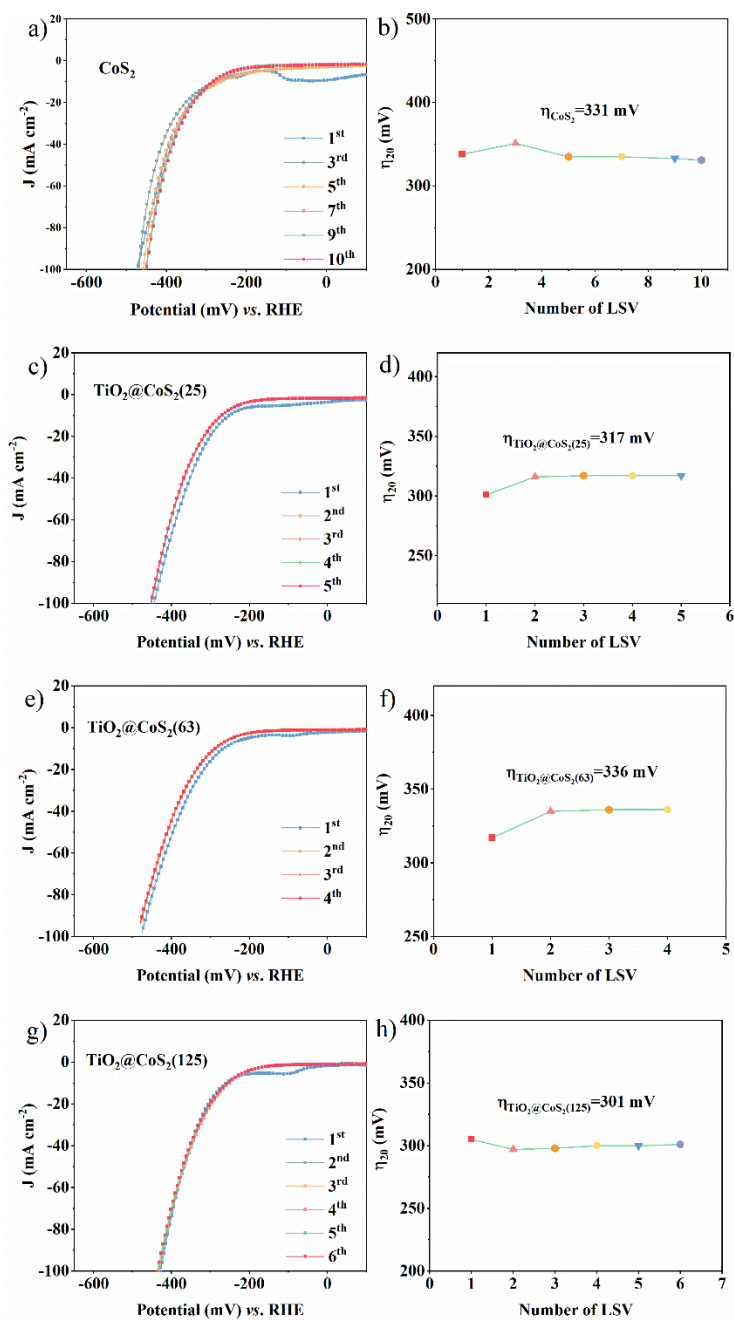
Figure S8. LSV curves of (a) pristine CoS2, (c) TiO2@CoS2(25), (e) TiO2@CoS2(63), and (g) TiO2@CoS2(125). Variation of η_{20} with the number of LSV scans corresponding to (b) pristine CoS2, (d) TiO2@CoS2(25), (f) TiO2@CoS2(63), and (h) TiO2@CoS2(125). The number in the brackets following the name of compounds is the ALD deposition cycle number.

**Table S2**. Performance of typical reported HER electrocatalysts in alkaline media.

Catalysts	η_{20} (mV)	Tafel slope (mV dec^{-1})	Electrolyte	Counter electrode
TiO$_2$@Co$_3$O$_4$ (this work)	49	79	1M KOH	Graphite rod
CoP/NiCoP/NC[39]	120	64	1M KOH	Graphite rod
CoP-InNC@CNT[40]	188	56	1M KOH	Graphite rod
Co-Fe-P[41]	110	66	1M KOH	Graphite rod
CoFe-PBA NS@NF-24[42]	100	66	1M KOH	Carbon rod
Co@N-CS/N-boHCP@CC[43]	101	65	1M KOH	Carbon rod
VN/Co–NC[44]	64	51	1M KOH	Graphite rod
Co@N-CNTs@rGO[45]	151	55	1M KOH	carbon rod
Co-B/Ni[46]	185	68	1M KOH	carbon rod
CoFeZr Oxides on NF[47]	120	119.3	1M KOH	graphite rod
Zn$_{0.30}$Co$_{2.70}$S$_4$[48]	101	47.5	1M KOH	graphite rod
NiCoP/rGO[49]	250	124.1	1M KOH	Pt wire
CoP NW[50]	330	105	1M KOH	Au foil
Co/NBC-900[51]	160	146	1M KOH	graphite rod
CoP/Co-MOF[52]	52	56	1M KOH	carbon rod
Co@CNF-700[53]	260	96	1M KOH	graphic rod
Co-MoS$_2$/BCCF-21[54]	65	52	1M KOH	carbon fiber cloth
Co/Co$_3$O$_4$[55]	129	44	1M KOH	Pt wire
Co-N-MoO$_2$[56]	338	126.8	0.1M KOH	carbon rod
CoP/CC[57]	59	42.6	1M KOH	graphite rod
Co-P/NC[58]	212	51	1M KOH	Pt wire
Co/Co$_9$S$_8$@SNGS1000[59]	370	96.1	0.1M KOH	platinum wire
PtSA–Co(OH)$_2$@Ag NW[60]	49	115.8	1M KOH	graphite sheet
2D-MoS$_2$/Co(OH)$_2$[61]	130	76	1M KOH	Graphite Rod
Mo-NiP$_x$/NiS$_y$[62]	110	73	1M KOH	carbon rod
PdPtCuNiP HEMG[63]	52	37.4	1M KOH	graphite rod
CoNi-inf[64]	110	57	1M KOH	graphite rod
Mo-Ni$_3$S$_2$/Ni$_x$P$_y$/NF[65]	128	68.4	1M KOH	graphite rod
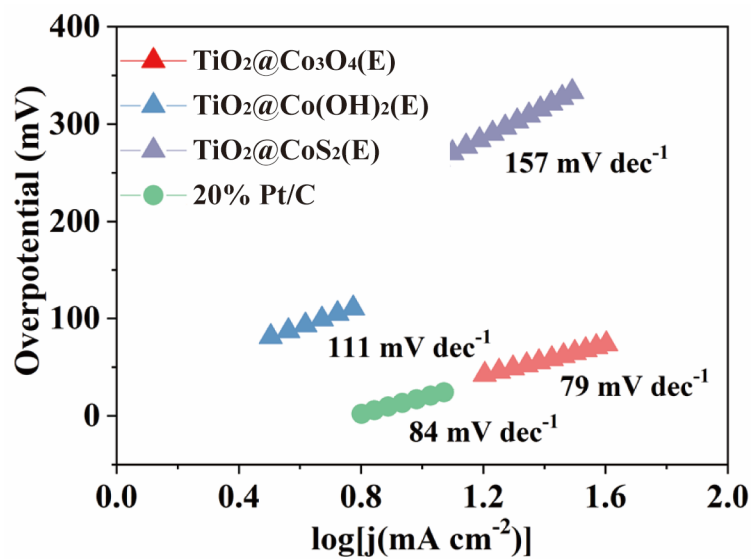
Figure S9. Tafel plot of TiO$_2$@Co$_3$O$_4$(E), TiO$_2$@Co(OH)$_2$(E), TiO$_2$@CoS$_2$(E), and Pt/C.
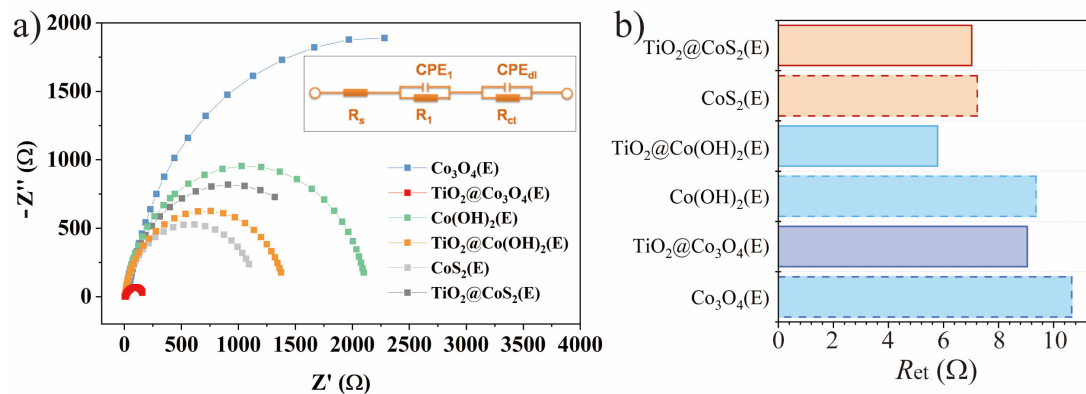
Figure S10. (a) Nyquist plot of the EIS spectra of comparative samples. (b) Comparison of R_{et} of comparative samples. Inset in (a) shows the equivalent circuit used for the data fitting of EIS spectra. R_s is the overall series resistance, CPE_1 and R_1 are the constant phase element and resistance describing electron transport at GCE/electrocatalyst interface, respectively, CPE_{dl} is the constant phase element of the electrocatalyst/electrolyte interface, and R_{ct} is the charge transfer resistance at electrocatalyst/electrolyte interface.

Table S3. Values of equivalent circuit elements resulted from fitting of EIS data.

Sample	R_s (Ω)	Q_{dl} (F S^{n-1})	n_{dl}	R_{ct} (Ω)	Q_1 (F S^{n-1})	n_1	R_1 (Ω)
Co$_3$O$_4$(E)	2.873	1.357E-4	0.8377	5540	1.438E-7	0.9747	7.783
TiO$_2$@ Co$_3$O$_4$(E)	2.992	7.743E-4	0.8276	173	7.963E-7	0.8653	6.053
CoS$_2$(E)	1.907	2.6E-3	0.9401	1161	2.787E-7	1	5.322
TiO$_2$@CoS$_2$(E)	2.457	4.2E-3	0.9286	1831	9.834E-7	0.9125	4.566
Co(OH)$_2$(E)	1.872	4.333E-5	0.9325	2124	2.624E-7	0.9999	7.488
TiO$_2$@Co(OH)$_2$(E)	2.512	1.44E-4	0.9236	1414	9.01E-7	0.9379	3.274
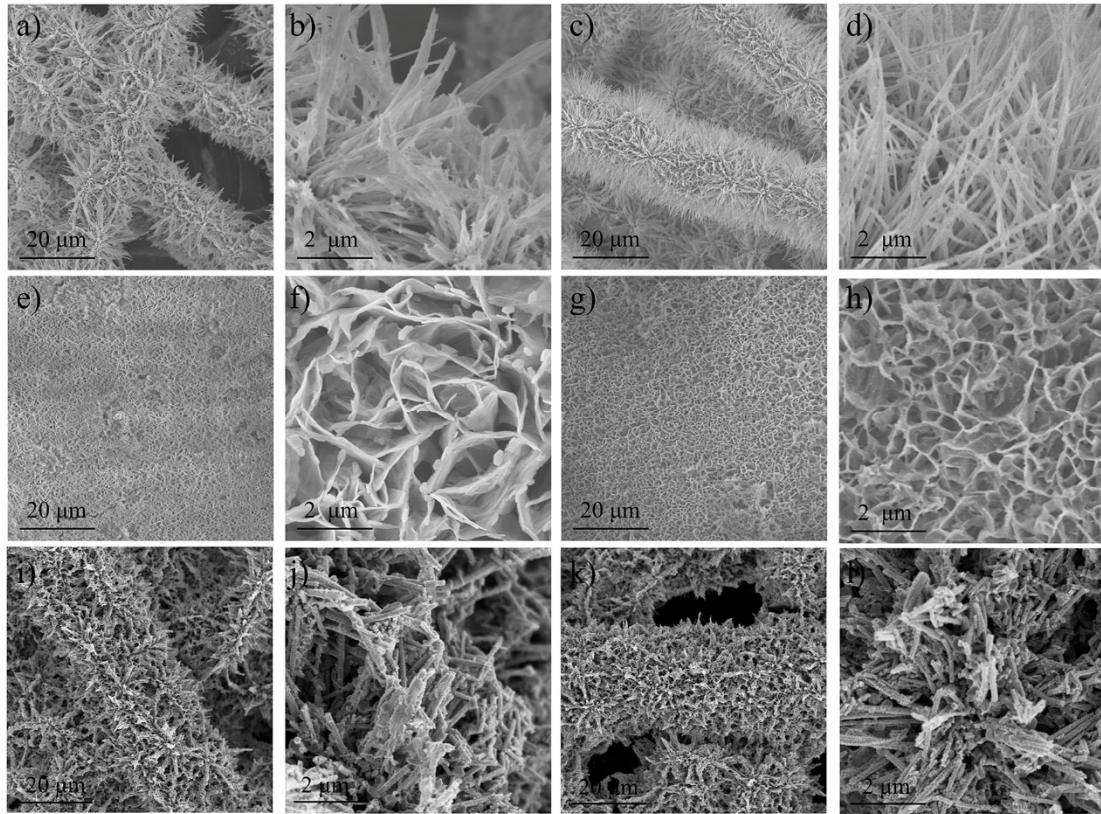
Figure S11. SEM images of measured samples: (a,b) $Co_3O_4(E)$, (c,d) $TiO_2@Co_3O_4(E)$, (e,f) $Co(OH)_2(E)$, (g,h) $TiO_2@Co(OH)_2(E)$, (i,j) $CoS_2(E)$, and (k,l) $TiO_2@CoS_2(E)$.
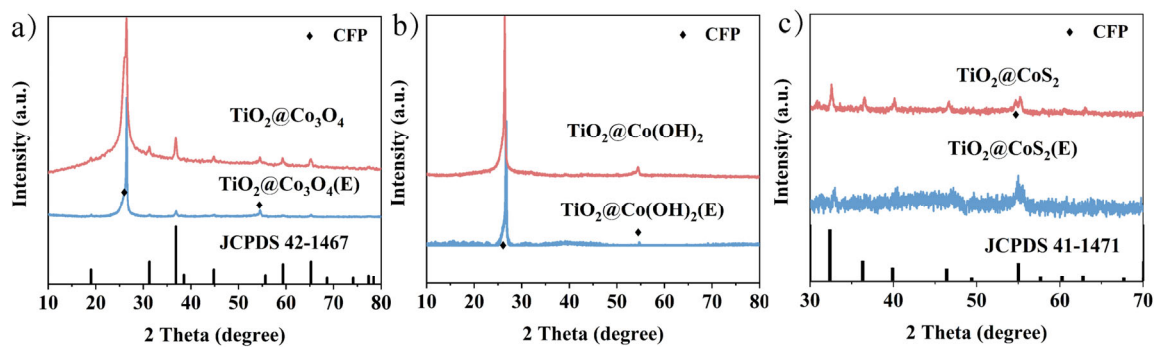
Figure S12. XRD of (a) TiO$_2$@Co$_3$O$_4$ and TiO$_2$@Co$_3$O$_4$(E), (b) TiO$_2$@Co(OH)$_2$ and TiO$_2$@Co(OH)$_2$(E), and (c) TiO$_2$@CoS$_2$ and TiO$_2$@CoS$_2$(E). It is worth noting that the XRD patterns of TiO$_2$@Co$_3$O$_4$, TiO$_2$@Co(OH)$_2$, and TiO$_2$@CoS$_2$ in Figure S12 are the same as that of corresponding samples in Figure S1. They are shown here again for the convenience of comparison.
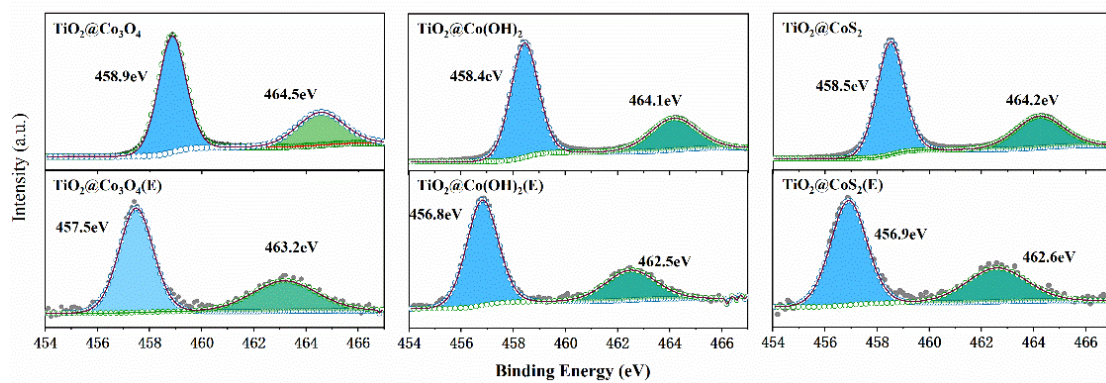
Figure S13. Ti 2p XPS spectra of TiO$_2$@Co$_3$O$_4$, TiO$_2$@Co$_3$O$_4$(E), TiO$_2$@Co(OH)$_2$, TiO$_2$@Co(OH)$_2$(E), TiO$_2$@CoS$_2$, and TiO$_2$@CoS$_2$(E).
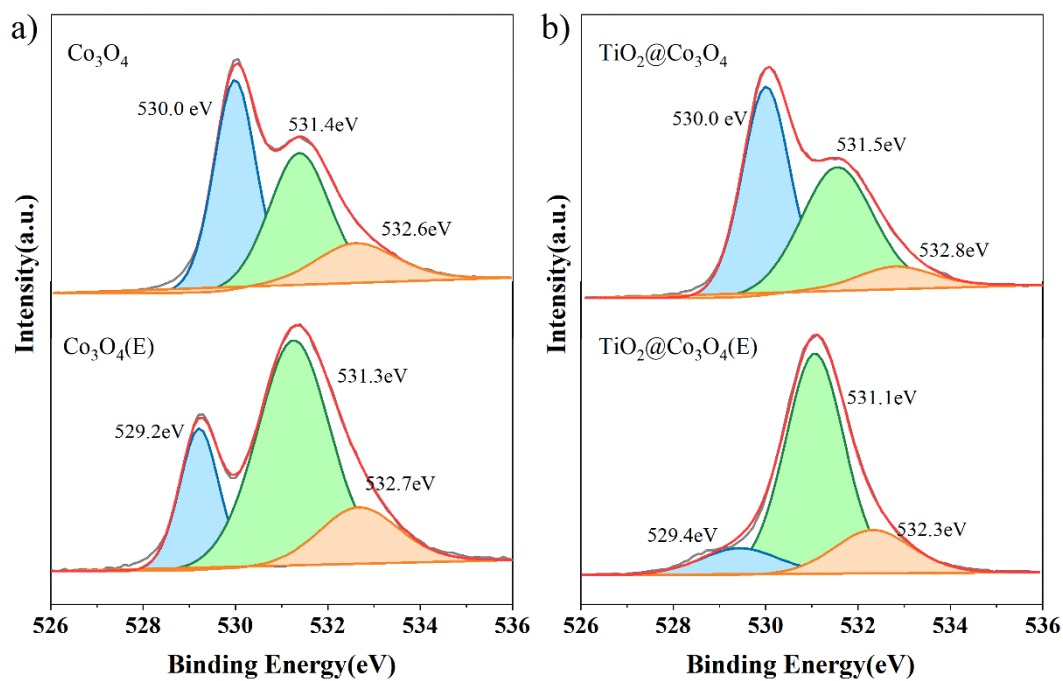
Figure S14. O 1s window XPS spectra for (a) Co_3O_4 and $Co_3O_4(E)$, and (b) $TiO_2@Co_3O_4$, and $TiO_2@Co_3O_4(E)$. The grey lines are experimental results, and the red lines are fitting envelopes. The filled peaks are fitting results.
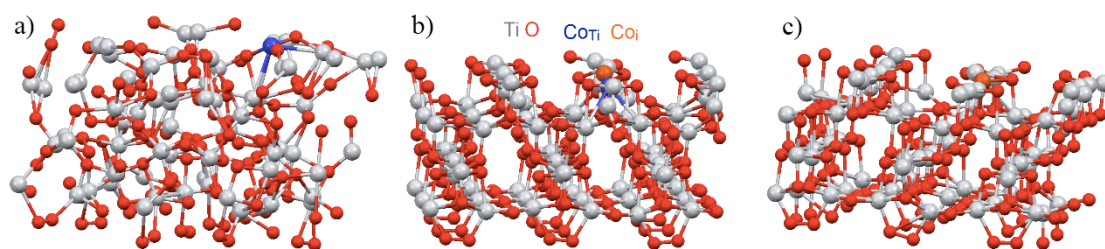
Figure S15. Optimized atomic structure of (a) the supercells of d-TiO$_2$ with a substitutional cobalt impurity, (b) (001) supercell of TiO$_2$ with a pair of substitutional and interstitial cobalt impurities and without oxygen vacancies, and (c) the same surface of a-TiO$_x$ with an interstitial cobalt impurity.

Table S4. Formation energies (in eV/Co) of realistic configurations of Co-defects in different titania hosts calculated for different sources of cobalt.

Source of Co	Co-defects configuration	Host		
		d-TiO$_2$	TiO$_2$	a-TiO$_x$
Co$_3$O$_4$	Co$_{Ti}$	+7.89	+4.03	+2.43
	Co$_{Ti}$+Co$_i$	+2.66	+2.24	+1.96
	Co$_i$	+1.77	+1.65	+1.22
Co(OH)$_2$	Co$_{Ti}$	+5.99	+2.13	+0.53
	Co$_{Ti}$+Co$_i$	+0.76	+0.34	+0.06
	Co$_i$	-0.13	-0.25	-0.68
CoS$_2$	Co$_{Ti}$	+1.87	-1.99	-3.59
	Co$_{Ti}$+Co$_i$	-3.36	-3.78	-4.06
	Co$_i$	-4.25	-4.37	-4.80

Table S5. Calculated enthalpies of the water decomposition processes described in equation 1, desorption of hydroxyl group from the surface of catalyst or co-catalyst to liquid media (eq. 2) and Tafel reaction (eq. 3), denoted as E_1, E_2, and E_T, respectively, for the various considered defects.

Row	Host	Configuration of Co-defects in TiO_2 matrixes	E_1, eV/H_2O	E_2, eV/OH^-	E_T, eV/H_2
1	Co_3O_4	without TiO_2	+1.92	-1.15	-0.76
	Co_3O_{4-x}		+2.09	-1.49	-0.24
2	d-TiO_2	undoped	-0.58	+1.49	+2.08
		+Co_{Ti}	+3.04	+0.38	-2.66
		+Co_{Ti}+Co_i	+3.17	-0.95	-3.90
		+Co_i	+3.58	-2.56	-4.14
3	TiO_2	undoped	+4.16	+1.22	-4.38
		+Co_{Ti}	+1.01	+1.45	+2.26
		+Co_{Ti}+Co_i	-2.40	-0.80	+0.67
		+Co_i	-1.82	-1.13	+0.60
4	a-TiO_x	undoped	-2.56	+3.18	+1.93
		+Co_{Ti}	+4.02	-3.06	-4.07
		+Co_{Ti}+Co_i	-0.35	-2.27	-1.92
		+Co_i	-1.95	-1.73	+0.22
5	Co_3O_4	@d-TiO_2	+2.25	+1.49	-0.76
		@TiO_2	-0.22	+1.22	-0.76
		@a-TiO_x	-0.42	+3.18	-0.76
		@TiO_2(Co_i)	-0.38	-1.13	-0.76
		@a-TiO_x(Co_i)	-0.97	-1.73	-0.76

References

1   C. Lv, X. Wang, L. Gao, A. Wang, S. Wang, R. Wang, X. Ning, Y. Li, D. W. Boukhvalov, Z. Huang and C. Zhang, *ACS Catal.*, 2020, **10**, 13323–13333.

2   R. T. Poole, P. C. Kemeny, J. Liesegang, J. G. Jenkin and R. C. G. Leckey, *J. Phys. F: Met. Phys.*, 1973, **3**, L46-L48.

3   H. Vrubel and X. Hu, *Angew. Chem. Int. Ed.*, 2012, **51**, 12703–12706.

4   Z. Lv, M. Tahir, X. Lang, G. Yuan, L. Pan, X. Zhang and J.-J. Zou, *J. Mater. Chem. A*, 2017, **5**, 20932–20937.

5   P. Xiao, M. A. Sk, L. Thia, X. Ge, R. J. Lim, J.-Y. Wang, K. H. Lim and X. Wang, *Energy Environ. Sci.*, 2014, **7**, 2624–2629.

6   D. Merki, S. Fierro, H. Vrubel and X. Hu, *Chem. Sci.*, 2011, **2**, 1262–1267.

7   F. H. Saadi, A. I. Carim, J. M. Velazquez, J. H. Baricuatro, C. C. L. McCrory, M. P. Soriaga and N. S. Lewis, *ACS Catal.*, 2014, **4**, 2866–2873.

8   M. Anwar, C. A. Hogarth and R. Bulpett, *J. Mater. Sci.*, 1990, **25**, 1784–1788.

9   K. T. Ng and D. M. Hercules, *J. Phys. Chem.*, 1976, **80**, 2094–2102.

10 Q. Li, L. Wang, X. Ai, H. Chen, J. Zou, G.-D. Li and X. Zou, *Chem. Commun.*, 2020, **56**, 13983–13986.

11 Y.-T. Xu, X. Xiao, Z.-M. Ye, S. Zhao, R. Shen, C.-T. He, J.-P. Zhang, Y. Li and X.-M. Chen, *J. Am. Chem. Soc.*, 2017, **139**, 5285–5288.

12 B. Ren, D. Li, Q. Jin, H. Cui and C. Wang, *J. Mater. Chem. A*, 2017, **5**, 19072–19078.

13 Z. Pu, X. Ya, I. S. Amiinu, Z. Tu, X. Liu, W. Li and S. Mu, *J. Mater. Chem. A*, 2016, **4**, 15327–15332.

14 Z. Liu, N. Li, C. Su, H. Zhao, L. Xu, Z. Yin, J. Li and Y. Du, *Nano Energy*, 2018, **50**, 176–181.

15 X. Wang, Y. Chen, B. Zheng, F. Qi, J. He, P. Li and W. Zhang, *Electrochimica Acta*, 2016, **222**, 1293–1299.

16 Jianou Shi, David L. Allara, *Langmuir*, 1996, **12**, 5099–5108.

17 P. Mills and J. L. Sullivan, *J. Phys. D: Appl. Phys.*, 1983, **16**, 723–732.

18 H. Li, P. Wen, Q. Li, C. Dun, J. Xing, C. Lu, S. Adhikari, L. Jiang, D. L. Carroll and S. M. Geyer, *Adv. Energy Mater.*, 2017, **7**, 1700513.

19 X. Fan, Z. Peng, R. Ye, H. Zhou and X. Guo, *ACS Nano*, 2015, **9**, 7407–7418.

20 Y. Wu, J. Cai, Y. Xie, S. Niu, Y. Zang, S. Wu, Y. Liu, Z. Lu, Y. Fang, Y. Guan, X. Zheng, J. Zhu, X. Liu, G. Wang and Y. Qian, *Adv. Mater.*, 2020, **32**, e1904346.

21 J. Kibsgaard, C. Tsai, K. Chan, J. D. Benck, J. K. Nørskov, F. Abild-Pedersen and T. F. Jaramillo, *Energy Environ. Sci.*, 2015, **8**, 3022–3029.

22 R. Miao, B. Dutta, S. Sahoo, J. He, W. Zhong, S. A. Cetegen, T. Jiang, S. P. Alpay and S. L. Suib, *J. Am. Chem. Soc.*, 2017, **139**, 13604–13607.

23 H. Zhang, L. Nengzi, B. Li, Q. Cheng, J. Gou and X. Cheng, *Renew. Energ. Renew. Energ.*, 2020, **155**, 717–724.

24 E. Paparazzo, *J. Electron. Spectros. Relat. Phenomena*, 1987, **43**, 97–112.

25 N. S. McIntyre, D. D. Johnston, L. L. Coatsworth, R. D. Davidson and J. R. Brown, *Surf. Interface Anal.*, 1990, **15**, 265–272.

26 J. Masa, P. Weide, D. Peeters, I. Sinev, W. Xia, Z. Sun, C. Somsen, M. Muhler and W. Schuhmann, *Adv. Energy Mater.*, 2016, **6**, 1502313.

27 Y. Chen, P. Sun and W. Xing, *J. Chem. Sci.*, 2019, **131**, 1–8.

28 E. J. Popczun, C. G. Read, C. W. Roske, N. S. Lewis and R. E. Schaak, *Angew. Chem. Int. Ed.*, 2014, **53**, 5427–5430.

29 M. S. Faber, R. Dziedzic, M. A. Lukowski, N. S. Kaiser, Q. Ding and S. Jin, *J. Am. Chem. Soc.*, 2014, **136**, 10053–10061.

30 D. Kong, H. Wang, Z. Lu and Y. Cui, *J. Am. Chem. Soc.*, 2014, **136**, 4897–4900.

31 K. S. Kim, *Phys. Rev. B*, 1975, **11**, 2177–2185.

32 V. Nemoshkalenko, V. Didyk, V. Krivitskii and A. Senkevich, *Zh. Neorg. Khim.*, 1983, **28**, 2182–2186.

33 P. Zhang, M. Wang, Y. Yang, T. Yao, H. Han and L. Sun, *Nano Energy*, 2016, **19**, 98–107.

34 J. Lai, B. Huang, Y. Chao, X. Chen and S. Guo, *Adv. Mater.*, 2019, **31**, e1805541.

35 Z. Huang, Z. Chen, Z. Chen, C. Lv, H. Meng and C. Zhang, *ACS Nano*, 2014, **8**, 8121–8129.

36 Q. Ma, C. Hu, K. Liu, S.-F. Hung, D. Ou, H. M. Chen, G. Fu and N. Zheng, *Nano Energy*, 2017, **41**, 148–153.

37 H. Zhou, Y. Wang, R. He, F. Yu, J. Sun, F. Wang, Y. Lan, Z. Ren and S. Chen, *Nano Energy*, 2016, **20**, 29–36.

38 V. I. Nefedov, M. N. Firsov and I. S. Shaplygin, *J. Electron. Spectros. Relat. Phenomena*, 1982, **26**, 65–78.

39 R. Boppella, J. Tan, W. Yang and J. Moon, *Adv. Funct. Mater*, 2019, **29**, 1807976.

40 L. Chai, Z. Hu, X. Wang, Y. Xu, L. Zhang, T.-T. Li, Y. Hu, J. Qian and S. Huang, *Adv.*

Sci., 2020, **7**, 1903195.

41 J. Chen, J. Liu, J.-Q. Xie, H. Ye, X.-Z. Fu, R. Sun and C.-P. Wong, *Nano Energy*, 2019, **56**, 225–233.

42 Z. Chen, B. Fei, M. Hou, X. Yan, M. Chen, H. Qing and R. Wu, *Nano Energy*, 2020, **68**, 104371.

43 Z. Chen, Y. Ha, H. Jia, X. Yan, M. Chen, M. Liu and R. Wu, *Adv. Energy Mater.*, 2019, **9**, 1803918.

44 Z. Chen, H. Qing, R. Wang and R. Wu, *Energy Environ. Sci.*, 2021, **14**, 3160–3173.

45 Z. Chen, R. Wu, Y. Liu, Y. Ha, Y. Guo, D. Sun, M. Liu and F. Fang, *Adv. Mater.*, 2018, **30**, 1802011.

46 W. Hao, R. Wu, R. Zhang, Y. Ha, Z. Chen, L. Wang, Y. Yang, X. Ma, D. Sun, F. Fang and Y. Guo, *Adv. Energy Mater.*, 2018, **8**, 1801372.

47 L. Huang, D. Chen, G. Luo, Y.-R. Lu, C. Chen, Y. Zou, C.-L. Dong, Y. Li and S. Wang, *Adv. Mater.*, 2019, **31**, e1901439.

48 Z.-F. Huang, J. Song, K. Li, M. Tahir, Y.-T. Wang, L. Pan, L. Wang, X. Zhang and J.-J. Zou, *J. Am. Chem. Soc.*, 2016, **138**, 1359–1365.

49 J. Li, M. Yan, X. Zhou, Z.-Q. Huang, Z. Xia, C.-R. Chang, Y. Ma and Y. Qu, *Adv. Funct. Mater*, 2016, **26**, 6785–6796.

50 W. Li, X. Gao, D. Xiong, F. Xia, J. Liu, W.-G. Song, J. Xu, S. M. Thalluri, M. F. Cerqueira, X. Fu and L. Liu, *Chem. Sci.*, 2017, **8**, 2952–2958.

51 M.-R. Liu, Q.-L. Hong, Q.-H. Li, Y. Du, H.-X. Zhang, S. Chen, T. Zhou and J. Zhang, *Adv. Funct. Mater*, 2018, **28**, 1801136.

52 T. Liu, P. Li, N. Yao, G. Cheng, S. Chen, W. Luo and Y. Yin, *Angew. Chem. Int. Ed.*, 2019, **58**, 4679–4684.

53 H. Su, H.-H. Wang, B. Zhang, K.-X. Wang, X.-H. Li and J.-S. Chen, *Nano Energy*, 2016, **22**, 79–86.

54 Q. Xiong, Y. Wang, P.-F. Liu, L.-R. Zheng, G. Wang, H.-G. Yang, P.-K. Wong, H. Zhang and H. Zhao, *Adv. Mater.*, 2018, **30**, 1801450.

55 X. Yan, L. Tian, M. He and X. Chen, *Nano Lett.*, 2015, **15**, 6015–6021.

56 L. Yang, J. Yu, Z. Wei, G. Li, L. Cao, W. Zhou and S. Chen, *Nano Energy*, 2017, **41**, 772–779.

57 X. L. Yang, A. Y. Lu, Y. H. Zhu, M. N. Hedhili, S. X. Min, K. W. Huang, Y. Han and L. J. Lin, *Nano Energy*, 2015, **15**, 634–641.

58 B. You, N. Jiang, M. Sheng, S. Gul, J. Yano and Y. Sun, *Chem. Mater.*, 2015, **27**, 7636–7642.

59 X. Zhang, S. Liu, Y. Zang, R. Liu, G. Liu, G. Wang, Y. Zhang, H. Zhang and H. Zhao, *Nano Energy*, 2016, **30**, 93–102.

60 K. L. Zhou, C. Wang, Z. Wang, C. B. Han, Q. Zhang, X. Ke, J. Liu and H. Wang, *Energy Environ. Sci.*, 2020, **13**, 3082–3092.

61 Z. Zhu, H. Yin, C.-T. He, M. Al-Mamun, P. Liu, L. Jiang, Y. Zhao, Y. Wang, H.-G. Yang, Z. Tang, D. Wang, X.-M. Chen and H. Zhao, *Adv. Mater.*, 2018, **30**, 1801171.

62 J. Wang, M. Zhang, G. Yang, W. Song, W. Zhong, X. Wang, M. Wang, T. Sun and Y. Tang, *Adv. Funct. Mater*, 2021, 2101532.

63 Z. Jia, K. Nomoto, Q. Wang, C. Kong, L. Sun, L.-C. Zhang, S.-X. Liang, J. Lu and J. J. Kruzic, *Adv. Funct. Mater*, 2021, 2101586.

64 X. Tan, S. Geng, Y. Ji, Q. Shao, T. Zhu, P. Wang, Y. Li and X. Huang, *Adv. Mater.*, 2020, **32**, e2002857.

65 X. Luo, P. Ji, P. Wang, R. Cheng, D. Chen, C. Lin, J. Zhang, J. He, Z. Shi, N. Li, S. Xiao and S. Mu, *Adv. Energy Mater.*, 2020, **10**, 1903891.